Applied Catalysis B: Environmental 142–143 (2013) 38–44

Contents lists available at SciVerse ScienceDirect

Applied Catalysis B: Environmental

journal homepage: www.elsevier.com/locate/apcatb

Electronic and optical performances of Si and Fe-codoped TiO_2 nanoparticles: A photocatalyst for the degradation of methylene blue

Yanming Lin[a,b], Zhenyi Jiang[a,*], Chaoyuan Zhu[b], Xiaoyun Hu[c], Xiaodong Zhang[a], Haiyan Zhu[a], Jun Fan[d], Sheng Hsien Lin[b,e]

[a] Institute of Modern Physics, Northwest University, Xi'an 710069, PR China
[b] Department of Applied Chemistry, Institute of Molecular Science and Center for Interdisciplinary Molecular Science, National Chiao-Tung University, Hsinchu 30050, Taiwan
[c] Department of Physics, Northwest University, Xi'an 710069, PR China
[d] School of Chemical Engineering, Northwest University, Xi'an 710069, PR China
[e] Institute of Atomic and Molecular Sciences, Academia Sinica, Taipei 106, Taiwan

ARTICLE INFO

Article history:
Received 26 February 2013
Received in revised form 23 April 2013
Accepted 28 April 2013
Available online 4 May 2013

PACS:
31.15.E–
71.15.Mb
71.20.–b

Keywords:
TiO_2
Codoping
Visible-light photocatalyst
Density functional theory

ABSTRACT

The effect of substitutional Si, Fe, and Si and Fe (co)doping on the electronic structure and optical properties of anatase and rutile TiO_2 have been investigated by the density functional theory. The calculated results indicate that Si doping TiO_2 will induce an obvious band gap narrowing by mixing O 2*p* with Si 3*p* states, and a series of impurity energy levels (Fe 3*d*) appear in edge of the VB and the CB through Fe doping. The synergistic effects of Si and Fe codoping can extend optical absorption edge, which leads to higher visible-light photocatalytic activities than pure and monodoped anatase TiO_2. Si and Fe-codoped TiO_2 nanoparticles was prepared by a sol–gel-solvothermal method, and the photocatalytic activity of TiO_2 nanoparticles was examined by measuring the rate of methylene blue decomposition. The experimental results show that Si and Fe-codoped TiO_2 sample exhibits better optical absorption performance and higher photocatalytic activities for the degradation of methylene blue than pure and monodoped TiO_2, which verifies the reliability of our calculated results.

© 2013 Elsevier B.V. All rights reserved.

1. Introduction

Solar energy is the most noteworthy among renewable and sustainable energy resources because it is a clean and unlimited resource of energy and has the global availability. In order to relieve the energy crises, environment pollution and global warming, utilization of solar energy using photocatalysts has been extensively studied [1–3]. Among all materials developed for photocatalytic applications, titanium dioxide (TiO_2) is shown to be most promising owing to its high efficiency, low cost, photostability and nontoxicity [4–8]. However, as an important functional semiconductor material, the universal applications of TiO_2 are restricted to ultraviolet (UV) light ($\lambda < 400$ nm) due to the wide band gap of TiO_2 (3.2 eV for anatase phase and 3.0 eV for rutile phase). To efficiently utilize solar energy, reducing the band gap of TiO_2 to make it photosensitive to visible light has become one of the most important goals in photocatalytic and photovoltaic applications.

In the past decades, considerable efforts have been devoted to modifying of the electronic structure of TiO_2-based materials. For example, doping with transition metals such as Ag, Fe, Cr, and Ni [9–12], for the sake of shifting the absorption edge of TiO_2 to visible light. However, the drawbacks of transition-metal-doped materials are attributed to their thermal instability, increase of carrier-recombination centers and the requirement of an expensive facility (e.g. ion implantation). An alternative method to decrease the band gap of TiO_2 can be achieved by substituting lattice oxygen with nonmetal elements such as C, N, Si, F, and I [13–17]. Among the nonmetal doping systems, Si-doping TiO_2 has been reported to be a good candidate due to its unique properties of high thermal stability, low carrier-recombination centers and narrowing the band gap of TiO_2, as Si 3*p* states can effectively mix with O 2*p* states, leading to an acceptor level above the valence band maximum [15,18–21].

A few latest researches show that different ions codoping into TiO_2 can further narrow its band gap and enhance its photocatalytic activity [22–28]. For instance, Li et al. reported the C/H-codoping produces significant band gap narrowing, which leads to higher visible-light photocatalytic efficiency than the C-doped anatase TiO_2 [23]. The research of Su et al. suggested that the codoping

* Corresponding author. Tel.: +86 29 88303491; fax: +86 29 88302331.
E-mail addresses: jiangzy@nwu.edu.cn, linymnwu@gmail.com (Z. Jiang).

0926-3373/$ – see front matter © 2013 Elsevier B.V. All rights reserved.
http://dx.doi.org/10.1016/j.apcatb.2013.04.061

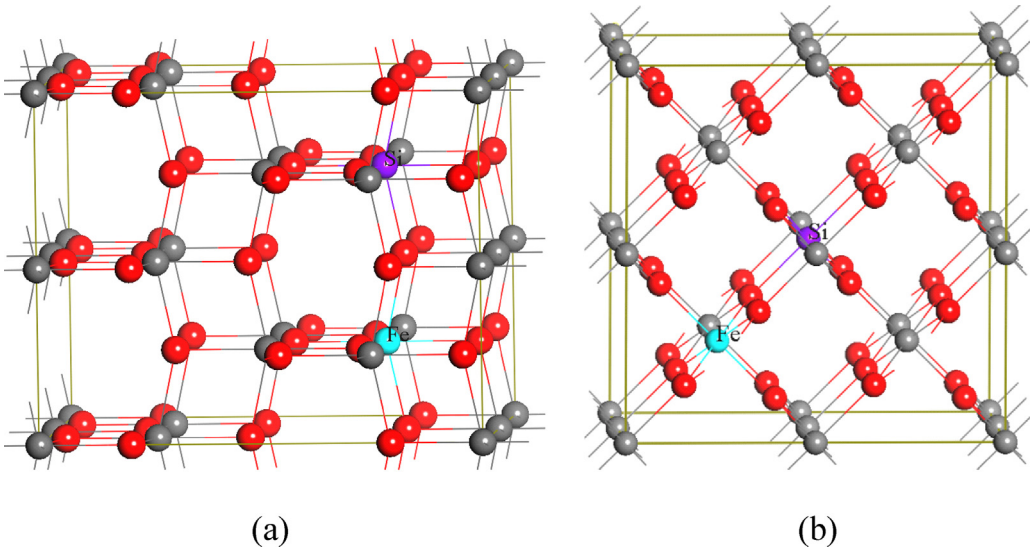

Fig. 1. Geometries of doping systems: (a) anatase supercell ($Ti_{16}O_{32}$) and (b) rutile supercell ($Ti_{16}O_{32}$). The atom doping sites are marked with Si and Fe. The gray spheres and red spheres represent the Ti and O atoms, respectively. The purple sphere and cyan sphere represent Si and Fe atom, respectively. (For interpretation of the references to color in this figure legend, the reader is referred to the web version of the article.)

of TiO_2 with N and Fe leads to the much narrowing of the band gap and greatly improves the photocatalytic activity under visible light irradiation [25]. Lv et al. reported the (Bi, C and N)-codoped TiO_2 nanoparticles [26]. It was found that the cation and the anion affect the properties of TiO_2 differently, and the order of photoreactivity for TiO_2 samples is as follow: (Bi,SCN)-TiO_2 > Bi-TiO_2 > undoped TiO_2 > P25 TiO_2 under UV- or visible-light illumination. Long et al. investigated systematically the band gap engineering of (N,Si)-codoped TiO_2 from hydrid density functional theory calculations [28]. The calculated results show that N and Si codoping can harvest longer-wavelength visible light than either those of N and Si monodoping, owing to the contribution from N 2*p* in the forbidden gap and Si 3*p* at the tail of the conduction band. These results indicate that codoping is one of the most effective approaches to extend the absorption edge to the visible light range in TiO_2. However, to the best of our knowledge, photocatalytic activity and optical absorption properties of Si and Fe-codoped TiO_2 for the degradation of methylene blue (MB) solution have no report on the theory and experiment. Therefore, the enhanced absorption of visible-light and photocatalytic activity are expected for Si and Fe-codoped TiO_2 material.

In this work, the electronic and optical performances of Si and Fe-codoped TiO_2 photocatalyst are studied using the density functional theory (DFT) to reveal the synergistic effects of Si and Fe codoping on the mechanism of band gap reducing and the origin of the enhanced visible-light photocatalytic activity. Nanocrystalline Si and Fe-codoped TiO_2 sample was successfully prepared by sol–gel-solvothermal method. It was found that the Si and Fe-codoped TiO_2 sample exhibited strong visible-light absorption and outstanding visible-light photocatalytic activity for the degradation of MB solution, which verified the reliability of our calculated results.

2. Calculational methods and experimental details

2.1. Computational details

The spin-polarized calculations were performed using the projector augmented wave (PAW) pseudopotentials as implemented in the VASP code [29,30]. The exchange correlation function was treated by the generalized gradient approximation (GGA) with the Perdew-Wang parameterization (known as GGA-PW91) [31]. The Brillouin-zone integrations were approximated by using the special k-point sampling of the Monhkorst-Pack scheme [32]. A cutoff energy of 500 eV and a mesh size of $5 \times 5 \times 5$ were used for geometry optimization and electronic structure calculations. Using the block Davidson scheme, both the atomic positions and cell parameters were optimized until the residual forces were below 0.01 eV/Å. In order to obtain the band gap that was consistent with the experimental result, the GGA + *U* method [33] was employed. The Coulombic interaction *U* and exchange energy *J* were set to be 10.0 eV and 1.0 eV, respectively. The calculated band gap of pure anatase TiO_2 was 2.9 eV, which was in good agreement with the experimental value [34].

The valence electron configurations considered in this study included Ti ($3d^24s^2$), O ($2s^22p^4$), Si ($3s^23p^2$), and Fe ($3d^64s^2$). All the (co)doped systems were constructed from a relaxed ($2 \times 2 \times 1$) 48-atom anatase and a relaxed ($2 \times 2 \times 2$) 48-atom rutile TiO_2 supercell, and shown in Fig. 1. As the position of Fe in the TiO_2 lattice was unclear, variety of positions of Fe atoms in the lattice were considered, such as substitutional Fe at the Ti site (Fe@Ti) and O site (Fe@O). In the Si-doped TiO_2, an Ti atom is substituted by an Si atom (Si@Ti) [6]. Similar substitutions were also considered for codoped systems, as Fe locates at either Ti or O site and Si locates at Ti site, namely, Si@Ti and Fe@Ti and Si@Ti and Fe@O.

2.2. Preparation of the photocatalyst

Nanocrystalline TiO_2 codoped with Si and Fe in this work was prepared by a sol–gel-solvothermal method. Tetrabutyl titanate ($[CH_3(CH_2)_3O]_4Ti$) was used as a starting material, tetraethyl orthosilicate ($(C_2H_5O)_4Si$) as a silicon source, and ferric nitrate hexahydrate ($Fe(NO_3)_3{\cdot}9H_2O$) as an iron source. All chemicals used in the experiments were of analytical reagent grade. Firstly, a desired amount (0.3367 g) of $Fe(NO_3)_3{\cdot}9H_2O$ was dissolved in 39.66 mL of glacial acetic acid (CH_3COOH) solution under stirring. Then, 5.58 mL of $(C_2H_5O)_4Si$ was dropwise added into the solution with stirring for 1 h. Secondly, 28.36 mL of $[CH_3(CH_2)_3O]_4Ti$ was also dropwise added into the solution with continuous stirring for 2 h, and the solution was transferred to a Teflon tube and placed in a 300 cm^3 stainless steel autoclave and the solution was heated in an oven and kept at 140 °C for 14 h. Thirdly, the precipitate obtained

was washed with ethanol and distilled water, respectively. Finally, the precipitate obtained was dried in a vacuum oven at 70 °C for 48 h. For comparison purposes, the samples of pure, Si-doped and Fe-doped TiO_2 were also prepared by similar procedures, respectively.

2.3. Characterizations

X-ray diffraction (XRD) patterns were recorded on a Rigaku D/MAX-2400 diffractometer with Cu *K*α radiation with λ = 0.154178 nm. The Brunauer–Emmett–Teller (BET) surface area of the samples were measured through nitrogen adsorption at 77 K (Nova 2000e). All the samples were degassed at 473 K for 4 h before the measurement. The UV–vis absorption spectra were obtained on an UV–vis spectrophotometer (UV-3600) equipped with an integrating sphere assembly, and using $BaSO_4$ as the reference sample. The spectra were recorded at room temperature in air within the range 300–800 nm.

2.4. Photocatalytic measurement

To evaluate the photocatalytic activity of samples, photocatalytic experiments were carried out in an inner-irradiation-type reactor. A cylindrical reaction cell was used to contain the reaction solution and a 500 W long-arc xenon lamp surrounded with a water cooling system was fixed in the center of the reaction cell. 0.2 g of photocatalyst was suspended in 200 mL of a methylene blue solution (20 mg/L) under stirring magnetically. The mixture was kept in the dark for 30 min to establish an adsorption–desorption equilibrium before the light radiation. The amount of MB in the solution was determined on the basis of its characteristic optical absorption at 665 nm using an UV–vis spectrophotometer based on Lambert-Beer's law.

3. Results and discussion

3.1. Optimized structure and defect formation energy

We performed structure optimization for the pure anatase and rutile TiO_2 supercell. For the anatase TiO_2, our calculated lattice parameters are $a = b = 3.774$ Å and $c = 9.409$ Å, which are in good agreement with the experimental values of $a = b = 3.782$ Å and $c = 9.502$ Å (within an error of 0.98%) [35]. For the rutile TiO_2, the calculated parameters of the unit cell are $a = b = 4.566$ Å and $c = 2.950$ Å, which are consistent with the experimental values of $a = b = 4.593$ Å and $c = 2.959$ Å (within an error of 0.59%) [35]. These results indicate that our calculation methods are reasonable, and the calculated results are authentic.

To probe the stabilities of the doped systems, we calculated the defect formation energy (E_f) for the doped and codoped systems according to the formulas

$$E_{f(X@Y)} = E_{(X@Y)} - E_{(Pure)} - (\mu_X - \mu_Y) \quad (1)$$

$$E_{f(Si@Y\&Fe@Y)} = E_{(Si@Y\&Fe@Y)} - E_{(Pure)} - (\mu_{S1} + \mu_{Fe} - \mu_Y - \mu_Y) \quad (2)$$

$(X = Si,\ Fe;\ Y = Ti,\ O)$

where $E_{(pure)}$ is the total energy of the host pure TiO_2 supercell, $E_{(X@Y)}$ and $E_{f(Si@Y\ and\ Fe@Y)}$ are the total energies of the supercells containing the impurities. For TiO_2, the chemical potentials of O and Ti satisfy the relation ships $\mu_{Ti} + 2\,\mu_O = \mu_{TiO2}$, $\mu_O \leq \mu_{O2/2}$, and $\mu_{Ti} \leq \mu_{Ti}^{metal}$. The chemical potential μ_O is determined by the energy of an O_2 molecule, μ_{Ti} is the energy of one Ti atom in the bulk Ti. μ_{Si} and μ_{Fe} are the chemical potentials of the Si and Fe impurities, which are calculated from the bulk Si and Fe, respectively. It should be noted that the smaller the E_f value, the more easily the impurity ions can be incorporated into the TiO_2 supercell. Our calculated formation energies for all doped and codoped TiO_2 are listed in Table 1. It can be observed that the formation energy of Fe@Ti and Si@Ti and Fe@Ti are much smaller than that of Fe@O and Si@Ti and Fe@O in Fe-doped and Si and Fe-codoped anatase TiO_2 under O-rich growth condition, and the formation energy of Fe@O and Si@Ti and Fe@O are much smaller than that of Fe@Ti and Si@Ti and Fe@Ti under Ti-rich growth condition, respectively. In particular, the formation energy of Fe@Ti and Si@Ti and Fe@Ti are negative values under O-rich growth condition, which indicates that the Si and Fe impurity are readily incorporated into the crystal. For the rutile TiO_2 system, the formation energy of Fe@Ti and Si@Ti and Fe@Ti are much smaller than that of Fe@O and Si@Ti and Fe@O in Fe-doped and Si and Fe-codoped systems under both O-rich and Ti-rich growth conditions. These results indicate that Si and Fe impurities are preferred to substitute the Ti ion in anatase and rutile TiO_2 systems under both Ti-rich and O-rich growth conditions, and Si@Ti and Fe@Ti TiO_2 photocatalyst has higher stability than other doped systems. Fig. 1(a) and (b) shows the corresponding anatase and rutile TiO_2 geometries, respectively.

Table 1
Defect formation energies of (co)doped anatase and rutile TiO_2 systems.

Doped systems		Defect formation energy (eV)			
		Anatase		Rutile	
		Ti-rich	O-rich	Ti-rich	O-rich
Doped	Si@Ti	1.1112	−9.1550	1.7109	−8.6382
	Si@O	5.8479	10.9810	6.1921	11.3667
	Fe@Ti	8.2451	−2.0211	7.4622	−2.8869
	Fe@O	7.8023	12.9354	9.8703	15.0449
Codoped	Si@Ti and Fe@Ti	8.4273	−12.1051	8.9740	−11.7242
	Si@O and Fe@O	10.0410	20.3072	15.5263	25.8755
	Si@Ti and Fe@O	6.6897	1.5566	9.9587	4.7842
	Si@O and Fe@Ti	10.3176	5.1845	11.4982	6.3237

3.2. Electronic structures

To study the effects of Si or/and Fe doping on the photocatalytic activity and optical absorption properties of anatase and rutile TiO_2, the electronic structures of all the (co)doping models are calculated. As the traditional DFT method seriously underestimated the band gap for semiconductors [35–37], we calculated the electronic structure using the DFT + *U* method, and the calculated band gap is 2.90 eV and 2.67 eV for anatase and rutile TiO_2, respectively. This calculated results are consistent with the experimental value of 3.20 eV for anatase structure [38] and 3.00 eV for rutile structure [39,40].

The total density of states (TDOS) and partial density of states (PDOS) of the (co)doping anatase TiO_2 are calculated and plotted in Fig. 2 for all the pure and doping anatase TiO_2 models, with up-spin DOS above zero and down-spin DOS below zero. For comparison, the TDOS and PDOS of pure anatase are also calculated, which indicate that the valence band (VB) mainly consists of the O 2*p* states with a large bandwidth, showing strong delocalization and bonding characteristic among the O 2*p* electrons, while the conduction band (CB) is mainly contributed by the Ti 3d states. In Si-doped anatase TiO_2 (Si@Ti), the VB broadens with the mixing of O 2*p* and Si 3*p* states, and the CB bottom has a decline about 0.15 eV, which can lead to a band gap narrowing. For Fe-doped anatase TiO_2 (Fe@Ti), it is shown that the band gap decreases by about 0.6 eV and most Fe 3*d* states are located in the band gap compared with the pure anatase TiO_2, which may be due to stronger interactions between the Fe 3*d* and Ti 3*d* orbitals. For Si and Fe-codoped anatase TiO_2 system (Si@Ti and Fe@Ti), some impurity states (Si 3*p* and Fe 3*d*) are

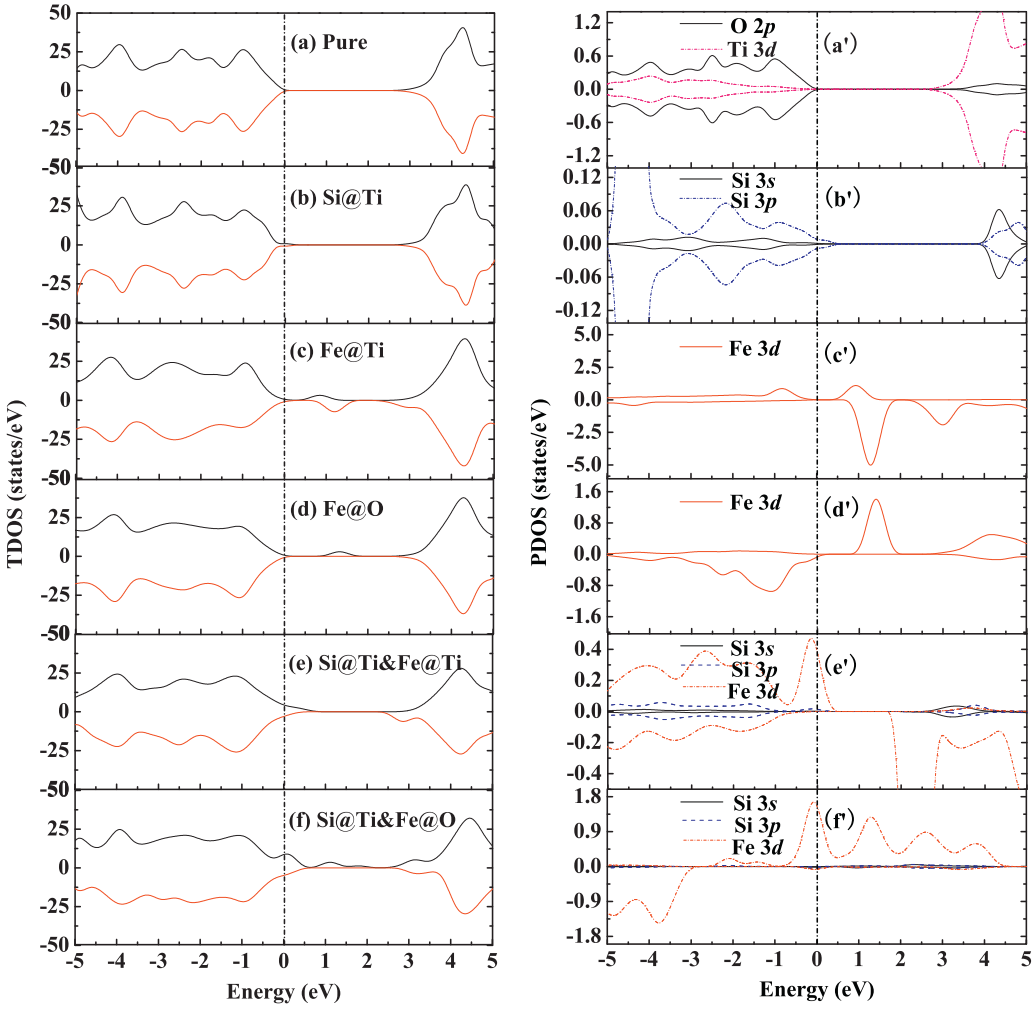

Fig. 2. Calculated TDOS and PDOS of different doping anatase TiO_2. The top of the valence band of pure anatase TiO_2 is taken as the reference level. Curves above and below the horizontal axis refer to the up-spin and down-spin DOS, respectively.

mixed with the VB and CB edge. The top of the VB has an obvious upward shift while the CB bottom has an obvious downward shift, which results in a band gap narrowing of about 1.0 eV compared with the pure anatase TiO_2. Thus, synergistic effect of Si and Fe codoping can lead to a decrease of the photon excitation energy and redshift the optical absorption edge to the visible-light range.

As in the case of (co)doping rutile TiO_2, the electronic structures of all the pure and doping rutile TiO_2 models were also calculated in order to investigate the Si and Fe doping effects on the optical absorption of rutile TiO_2. The TDOS and PDOS of all the models are shown in Fig. 3, with up-spin DOS above zero and down-spin DOS below zero. For pure rutile TiO_2, the VB is mainly contributed by the O 2*p* state, while the CB is mainly contributed by the Ti 3*d* state, as shown in Fig. 3(a) and (a'). The calculated band gap value is 2.67 eV, which is similar to other theoretical results [41,42]. For Si-doped rutile TiO_2 (Si@Ti), the VB broadens with the coupling of O 2*p* and Si 3*p* states, and the top of the VB has a rise about 0.12 eV compared with pure rutile TiO_2. These results lead to a band gap narrowing. For Fe-doped rutile TiO_2 (Fe@Ti), the top of the VB has a rise about 0.3 eV with the mixing of Fe 3*d* and O 2*p* states. Compared with the pure rutile TiO_2, the CB bottom has a decline about 0.11 eV with the coupling of Fe 3*d* and Ti 3*d* states. Consequently, Fe doping can further reduce the energy needed for electrons to be excited from the VB to the CB, which may be responsible for the redshift phenomena of optical absorption edge in Fe-doped TiO_2. For Si and Fe-codoped rutile TiO_2 (Si@Ti and Fe@Ti), the top of the VB also has a rise about 0.48 eV with the coupling of Si 3*p*, Fe 3*d* and O 2*p* states. And the bottom of the CB has a decline about 0.23 eV with the mixing of Fe 3*d* down-spin state and Ti 3*d* state. These results may induce an obvious redshift of the optical absorption edge in Si and Fe-codoped TiO_2.

Therefore, synergistic effects of Si and Fe codoping lead to a decrease of the photon excitation energy from the VB to the CB, which may induce more significant redshift of the absorption spectra edge. The calculated results indicate that Si and Fe codoping may lead to an outstanding photocatalytic activity in TiO_2 material.

3.3. Optical properties

According to the obtained electronic structures, we calculated the complex dielectric function $\xi = \xi_1 + i\xi_2$. The dielectric function can be defined in terms of current and field, which is most applicable for conductivity and optical responses. The corresponding absorption spectrum was estimated by the following equation

$$I(\omega) = 2\omega \left(\frac{(\xi_1^2(\omega) + \xi_2^2(\omega))^{1/2} - \xi_1(\omega)}{2} \right)^{1/2} \quad (3)$$

where I is the optical absorption coefficient, ω is the angular frequency ($E = \hbar\omega$).

The absorption spectrum of the pure and doping TiO_2 systems are calculated and shown in Fig. 4. In anatase TiO_2 (see Fig. 4(a)), it is

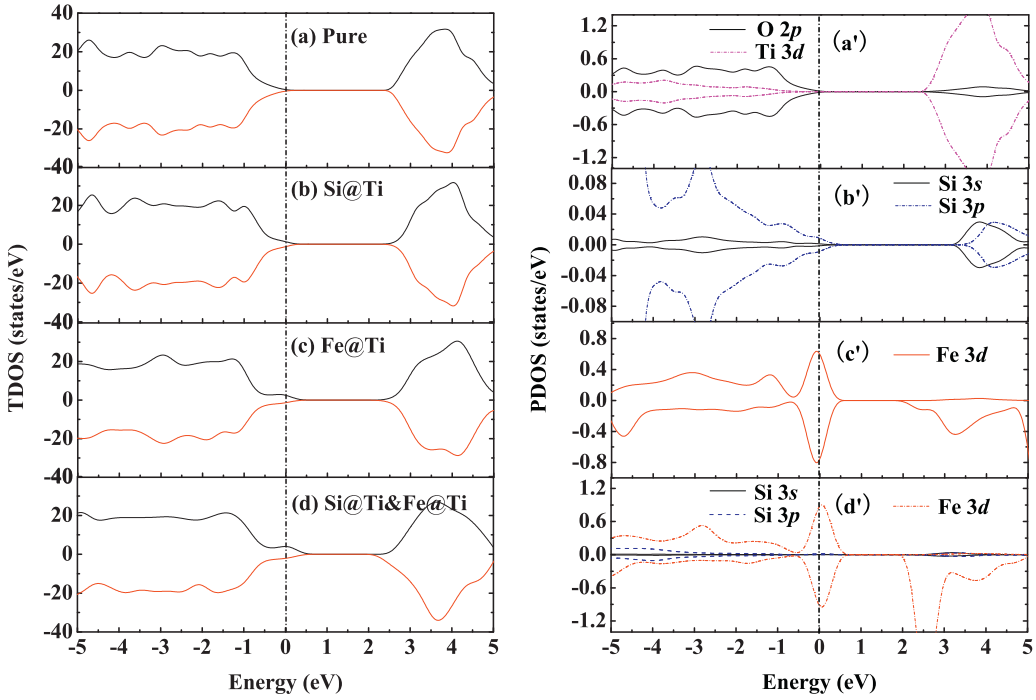

Fig. 3. Calculated TDOS and PDOS of different doping rutile TiO_2. The top of the valence band of pure rutile TiO_2 is taken as the reference level. Curves above and below the horizontal axis refer to the up-spin and down-spin DOS, respectively.

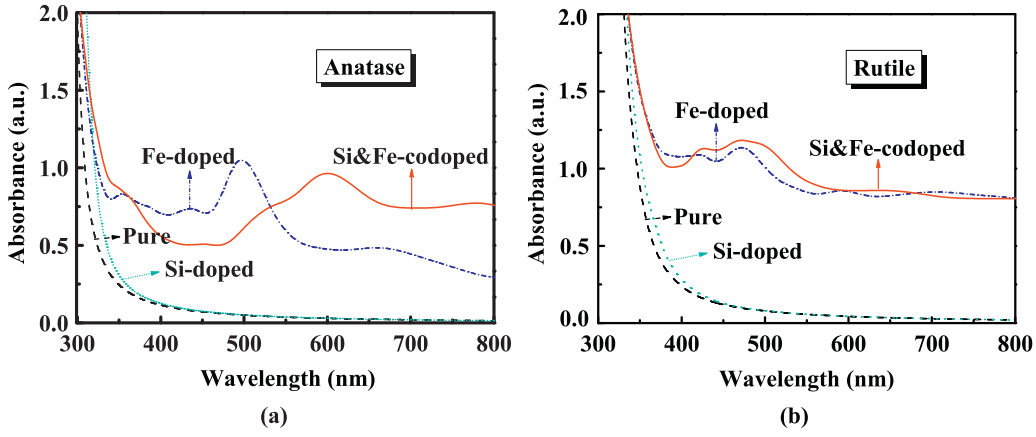

Fig. 4. The optical absorption spectra of pure and doping TiO_2 models: (a) anatase phase, and (b) rutile phase.

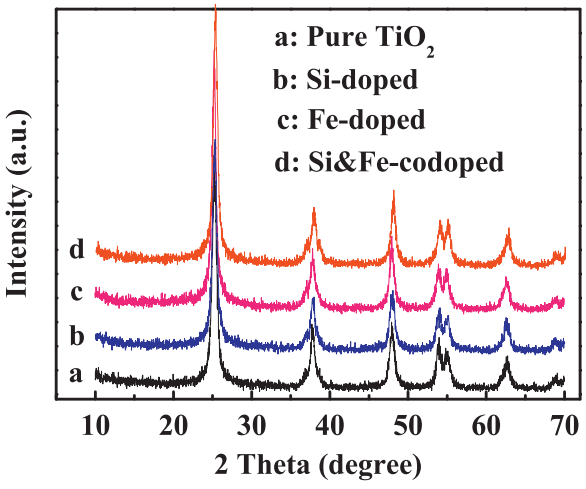

Fig. 5. XRD patterns for the pure and doping TiO_2 samples.

found that pure anatase TiO_2 can only respond to the UV-light and show no absorption activity in the visible-light region. For Si-doped system, it is clear that the narrowed band gap induces the increasing optical absorption in the UV-light region. For Fe-doped system, there are a series of impurity states (Fe 3*d* orbital) appearing in the band gap and the band gap has an obvious narrowing, which leads to a good optical absorption in the visible-light region. For Si and Fe-codoped TiO_2 system, synergistic effect of Si and Fe codoping induces a band gap narrowing, which lead to a decrease of the photon excitation energy in the view of electronic structure. It is also found that the pure rutile TiO_2 (Fig. 4(b)) can only respond to the UV-light and shows no absorption performance in the visible-light region. For Si doping system, with the coupling of O 2*p* and Si 3*p* states, the narrowed band gap induces the increasing optical absorption in the UV-light region. For Fe doping system, there are some impurity states (Fe 3*d* states) appearing in the edge of the VB and the CB. Thus, the electron transition from these impurity states to the CB would lead to an obvious reduction of absorption energy, which enhances the visible-light absorption for Fe-doped

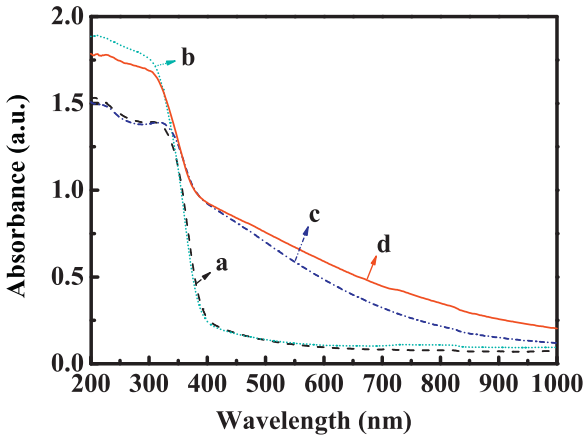

Fig. 6. UV–vis absorption spectra of (a) pure, (b) Si-doped, (c) Fe-doped, and (d) Si and Fe-codoped TiO_2 samples.

TiO_2. For Si and Fe-codoped system, it is obvious that the Si and Fe-codoped TiO_2 has a strong visible-light absorption in the range of 420–680 nm, which is due to decrease energy needed for electrons to be excited from the VB to the CB with synergistic effect of Si and Fe codoping. Therefore, Si and Fe codoping may lead to an excellent visible-light photocatalytic activity in TiO_2 material.

3.4. Characterization of the samples

Fig. 5 illustrates the XRD patterns for pure anatase TiO_2, Si-doped, Fe-doped and Si and Fe-codoped TiO_2 samples. It is found that almost all of the diffraction peaks are contributed by the anatase TiO_2 phase and no other visible impurity peak can be distinguished in the pattern of pure or doped sample. The BET surface areas for pure, Si-, Fe-, and Si and Fe-codoped TiO_2 are 84.21, 252.42, 226.72 and 308.31 m^2/g, respectively. It is shown that the surface area of TiO_2 powders is increased to 308.31 m^2/g with the coexistence of Si and Fe in TiO_2, about four times of that of pure TiO_2 powders.

The optical absorption spectra of the pure and doping systems are also measured by experiments, and shown in Fig. 6. Compared with the pure TiO_2, it is clear that the incorporation of Si into TiO_2 lattice induces the enhanced optical absorption in the UV-light region. For Fe-doped system, it exhibits an excellent absorption activity in the visible-light region. For Si and Fe-codoped TiO_2, it is obvious that the optical absorption in the UV–vis region is stronger than that of pure TiO_2, especially in the visible-light region. Therefore, the enhancement of absorption in the visible-light region can promote the utilization of the solar light, which may be responsible for the redshift of optical absorption edge and the outstanding photocatalytic activity in Si and Fe-codoped anatase TiO_2. However, there are small misalignments between the experimental and theoretical results, which may be due to neglect of the anisotropy of the absorption coefficient and the well-known limitation of DFT. But, from the perspective of qualitative analysis, the experimental results are consistent with the calculations.

3.5. Photocatalytic activity

The photocatalytic activity of the undoping and doping TiO_2 samples were evaluated by monitoring the degradation of MB, as shown in Fig. 7. The "Dark environment" shows that MB almost cannot be degraded using catalysts without the visible-light irradiation. The 'Blank' shows that MB almost cannot be degraded under the visible-light irradiation without catalysts, indicating that the photolysis can be ignored. The Si- and Fe-doped samples present the better photocatalytic activity compared with the pure TiO_2. This is because Si doping can reduce the band gap of TiO_2, while the impurity states of Fe 3*d* is also easy to appear in the forbidden gap of TiO_2. For Si and Fe-codoped TiO_2 sample (see Fig. 7), it has the best photocatalytic activity compared with the pure, Si-, Fe-doped TiO_2 samples, which is due to the enhanced optical absorption of visible and UV-light through Si and Fe codoping. Therefore, the Si and Fe-codoped TiO_2 sample exhibits best photocatalytic activity than the pure, Si-, Fe-doped TiO_2 samples.

4. Conclusion

In conclusion, we have investigated the electronic and optical performances of pure, Si-doped, Fe-doped, Si and Fe-codoped anatase and rutile TiO_2 based on DFT calculations. Our calculated results show that Si doping TiO_2 will induce an obvious band gap narrowing by mixing O 2*p* with Si 3*p* states, and there are a series of impurity energy states (Fe 3*d*) appearing in edge of the VB and the CB through Fe doping. The synergistic effects of Si and Fe codoping may further reduce the electrons excited energy from the VB to the CB under the visible-light irradiation, which enhances the photocatalytic activity and the redshift of absorption edge. The photocatalytic and optical absorption properties obtained by experiments reveal that Si and Fe-codoped TiO_2 sample exhibits better optical absorption performance and higher photocatalytic activities for the degradation of methylene blue than pure and monodoped TiO_2, which verifies the reliability of our calculated results.

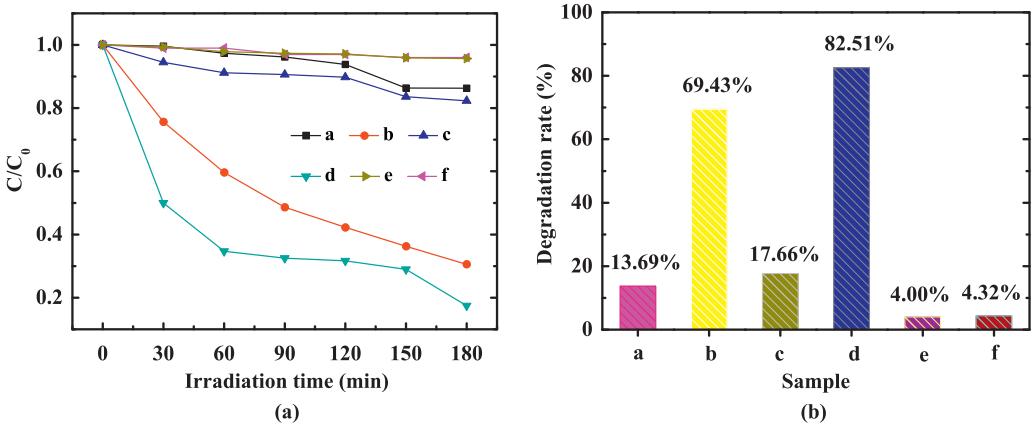

Fig. 7. Photocatalytic degradation rate of MB test during irradiation with visible-light radiation: (a) MB concentration changes as a function of irradiation time and (b) the comparison of degradation rate after 3 h of visible-light radiation. In figures, a: pure TiO_2, b: Si-doped, c: Fe-doped, d: Si and Fe-codoped, e: blank, f: dark environment.

Acknowledgements

Yanming Lin would like to thank Dr. Kesong Yang and Dr. Run Long for helpful discussions. This work was supported by the National Natural Science Foundation of China under Grants (Nos. 10647008, 50971099, and 21176199), the Research Fund for the Doctoral Program of Higher Education (Nos. 20096101110017 and 20096101110013), Key Project of Natural Science Foundation of Shaanxi Province of China (Nos. 2010JZ002 and 2011JM1001), and Graduate's Innovation Fund of Northwest University of China (No. YZZ12082).

References

[1] M. Grätzel, Nature 414 (2001) 338–344.
[2] V.B.R. Boppana, R.F. Lobo, Journal of Catalysis 281 (2011) 156–168.
[3] M.D. Hernandez-Alonso, F. Fresno, S. Suarez, J.M. Coronado, Energy and Environmental Science 2 (2009) 1231–1257.
[4] A. Fujishima, K. Honda, Nature 238 (1972) 37–38.
[5] R. Asahi, T. Morikawa, T. Ohwaki, K. Aoki, Y. Taga, Science 293 (2001) 269–271.
[6] S.U.M. Khan, M. Al-Shahry, W.B. Ingler Jr., Science 297 (2002) 2243–2245.
[7] Y. Lin, Z. Jiang, C. Zhu, X. Hu, X. Zhang, H. Zhu, J. Fan, Applied Physics Letters 101 (2012) 062106–062110.
[8] C.S. Chou, M.G. Guo, K.H. Liu, Y.S. Chen, Applied Energy 92 (2012) 224–233.
[9] S. Rodrigues, K.T. Ranjit, S. Uma, I.N. Martyanov, K.J. Klabunde, Advanced Materials 17 (2005) 2467–2471.
[10] R. Dholam, N. Patel, M. Adami, A. Miotello, International Journal of Hydrogen Energy 34 (2009) 5337–5346.
[11] R. Van Grieken, J. Marugan, C. Sordo, P. Martinez, C. Pablos, Applied Catalysis B: Environmental 93 (2009) 112–118.
[12] Y.M. Lin, Z.Y. Jiang, C.Y. Zhu, X.Y. Hu, X.D. Zhang, J. Fan, Materials Chemistry and Physics 133 (2012) 746–750.
[13] F. Dong, S. Guo, H. Wang, X.F. Li, Z.B. Wu, Journal of Physical Chemistry C 115 (2011) 13285–13292.
[14] K.M. Parida, B. Naik, Journal of Colloid and Interface Science 333 (2009) 269–276.
[15] K. Yang, Y. Dai, B. Huang, Chemical Physics Letters 456 (2008) 71–75.
[16] W. Ho, J.C. Yu, S. Lee, Chemical Communications 0 (2006) 1115–1117.
[17] X.T. Hong, Z.P. Luo, J.D. Batteas, Journal of Solid State Chemistry 184 (2011) 2244–2249.
[18] S.M. Oh, S.S. Kim, J.E. Lee, T. Ishigaki, D.W. Park, Thin Solid Films 435 (2003) 252–258.
[19] X. Yan, J. He, D.G. Evans, X. Duan, Y. Zhu, Applied Catalysis B: Environmental 55 (2005) 243–252.
[20] H. Ozaki, S. Iwamoto, M. Inoue, Chemistry Letters 34 (2005) 1082–1083.
[21] H. Ozaki, S. Iwamoto, M. Inoue, Catalysis Letters 113 (2007) 95–98.
[22] Y. Lin, Z. Jiang, C. Zhu, X. Hu, X. Zhang, H. Zhu, J. Fan, S.H. Lin, Journal of Materials Chemistry A 1 (2013) 4516–4524.
[23] N. Li, K.L. Yao, L. Li, Z.Y. Sun, G.Y. Gao, L. Zhu, Journal of Applied Physics 110 (2011) 073513–073517.
[24] P.P. González-Borrero, H.S. Bernabé, N.G.C. Astrath, A.C. Bento, M.L. Baesso, M.V. Castro Meira, J.S. De Almeida, A. Ferreira da Silva, Applied Physics Letters 99 (2011) 221909–221911.
[25] Y. Su, Y. Xiao, Y. Li, Y. Du, Y. Zhang, Materials Chemistry and Physics 126 (2011) 761–768.
[26] K. Lv, H. Zuo, J. Sun, K. Deng, S. Liu, X. Li, D. Wang, Journal of Hazardous Materials 161 (2009) 396–401.
[27] G.G. Nakhate, V.S. Nikam, K.G. Kanade, S. Arbuj, B.B. Kale, J.O. Baeg, Materials Chemistry and Physics 124 (2010) 976–981.
[28] R. Long, N.J. English, New Journal of Physics 14 (2012) 053007–053017.
[29] G. Kresse, J. Hafner, Physical Review B 49 (1994) 14251–14269.
[30] G. Kresse, J. Furthmüller, Physical Review B 54 (1996) 11169–11186.
[31] J.P. Perdew, C.J. Ahevary, S.H. Vosko, K.A. Jackson, M.R. Pederson, D.J. Singh, C. Fiolhais, Physical Review B 46 (2004) 6671–6687.
[32] H.J. Monkhorst, J.D. Pack, Physical Review B 13 (1976) 5188–5192.
[33] S.L. Dudarev, G.A. Botton, S.Y. Savarsov, C.J. Humphreys, A.P. Sutton, Physical Review B 57 (1998) 1505–1509.
[34] H. Tang, F. Lévy, H. Berger, P.E. Schmid, Physical Review B 52 (1995) 7771–7774.
[35] C. DiValentin, G. Pacchioni, A. Selloni, Physical Review B 70 (2004) 085116–085119.
[36] H. Weng, J. Dong, T. Fukumura, M. Kawasaki, Y. Kawazoe, Physical Review B 73 (2006), 121201(R)-121204. (R).
[37] R. Janisch, N.A. Spaldin, Physical Review B 73 (2006) 035201–035207.
[38] H. Tang, H. Berger, P.E. Schmid, F. Lévy, G. Burri, Solid State Communications 87 (1993) 847–850.
[39] J. Pascual, J. Camassel, H. Mathieu, Physical Review Letters 39 (1977) 1490–1493.
[40] J. Pascual, J. Camassel, H. Mathieu, Physical Review B 18 (1978) 5606–5614.
[41] Y. Lin, Z. Jiang, X. Hu, X. Zhang, J. Fan, Applied Physics Letters 100 (2012) 102105–102108.
[42] K. Yang, Y. Dai, B. Huang, M.H. Whangbo, Journal of Physical Chemistry C 113 (2009) 2624–2629.